Study on wheel polygonization of a metro vehicle based on polygonal wear simulation

Bin Fu [1]*, Stefano Bruni [1], Shihui Luo [2]

[1] Dipartimento di Meccanica, Politecnico di Milano, Via La Masa 1, Milano, 20156, Italy

[2]State Key Laboratory of Traction Power, Southwest Jiaotong University, Chengdu, 610031, China

[*] E-mail: bin.fu@polimi.it

Abstract: A long-term iterative wear model is proposed to predict the development of polygonal wear of railway wheels. To improve the simulation accuracy, the time step for numerical integration, wheel profile updating strategy and curve fitting methods are analysed. Then a metro vehicle with 8^{th} to 9^{th} order polygonal wheel is presented as a case study where critical vehicle speeds leading to a peculiar growth of wheel polygonization is identified by simulation and validated through field tests. Based on the simulated polygonal wear evolutions and analyses on vehicle vibrations, the mechanism of wheel polygonization is explained. Finally, two new strategies to investigate wheel polygonization are proposed.

Keywords: polygonal wear; metro; iterative long-term wear; resonance speed

1. Introduction

Polygonal wheels are observed in a broad range of railway vehicles, including metro vehicles [1,2], high-speed vehicles [3-4], locomotives [5] and freight wagons [6]. They are cause of increased dynamic forces and impacts at wheel-rail contact that have been investigated widely by means of simulation and field tests [7-9] and produce a very significant increase of vibration both in the vehicles and in the track, especially in vertical direction, ultimately resulting in reduced ride comfort, increase of noise and shorter life cycles of rails and vehicles. The explanation of the mechanism and causes for the formation and growth of wheel polygonization has challenged many researchers and still represents an open problem in railway engineering.

Some previous work [1,3,10] studied the relationship between bending resonances of wheelset and the development of polygonal wheel wear in high-speed vehicles, locomotives and metro vehicles. In fact, one mechanism proposed for wheel polygonization is based on the excitation of resonances in the vehicle and the track [4,11]. Other factors deemed to possibly affect the formation and growth of polygonal are the effects of wheel mass unbalance, inhomogeneity of wheel material properties, re-profiling tolerances. Due to the many factors potentially affecting the problem, systematic consensus on the causes of wheel polygonization has not been reached so far and a comprehensive understanding of the mechanism and remedies for this phenomenon is still lacking.

The various attempts proposed to explain wheel polygonization generally share a similar approach where a resonance frequency from the vehicle/track system is excited by the polygonal wheel and a wavelength fixing mechanism leads to the selective growth of some particular wavelengths of corrugation in the circumferential profile of the wheel. In these studies, the variation of the vehicle speed is often neglected or regarded as a minor effect, but it is an important and indispensable factor to get the excitation frequency from polygonal wheels, because in real operation the vehicle is seldom running at constant speed, so it may be difficult to identify the speed regimes actually leading to wheel polygonization.

This effect is particularly crucial for metro vehicles which are operated according to a speed profile characterised by frequent accelerations and decelerations.

One of the primary barriers to investigating wheel polygonization is the difficulty to define a comprehensive numerical model for the formation and growth of polygonal wear, capable to simulate the initiation phase and the subsequent polygonal wear evolution process. This requires that a short-term model for vehicle dynamics and train-track interaction is coupled to a long-term model of wheel wear, representing the evolution of polygonal wear on the surface of the wheel. The short-term model works on a timescale of some seconds and should be able to describe motion components happening at frequencies in the order of hundreds of Hz, i.e. with periods of oscillation of few milli-seconds. The formation of polygonal wear requires weeks or months to take place, so there can be 6 orders of magnitude difference in the times involved in the model. Establishing such a model requires therefore that suitable simplifying assumptions are made, whose impacts on the model's accuracy are discussed in this paper. Once the simulation model is available, wheel polygonization can be analysed quantitatively and a growth mechanism can be proposed and compared with field tests, which is the second main aim for this paper.

The paper is organised as follows. In Section 2, we propose an iterative simulation approach in which a wear model is used to calculate wear depth along the wheel circumference after each short-term simulation and Fourier series expansion function is used to smoothen the curve. To ensure the accuracy of the model, three important simulation settings are investigated in Section 3: the time step for numerical integration, the method for smoothing the worn profile and wheel profile updating strategy. In Section 4, a case study of a real metro vehicle with 8^{th} to 9^{th} order polygonal wheels is presented. In this case study, the simulation work and field tests lead us to identify a 'resonance speed' at which a peculiar growth of wheel polygonization takes place. Based on the simulation on wear evolution and the case study of the metro vehicle, new general strategies for investigating the wheel polygonization are summarized in Section 5. Finally, Section 6 provides a concise discussion of the results obtained and the final conclusions.

2. Simulation model for polygonal wear of railway wheels

2.1. Assumptions and a general scheme for polygonal wear model

The long-term iterative wear model in this work is based on three assumptions. Firstly, in a single short-term calculation, the variation of wheel and rail profiles is negligible, so that the wheel and rail profiles are assumed to be constant. The second assumption named multiple timescale means that scaling coefficients are applied to the short-term simulation to simulate wear effects taking place over a much longer timescale. The third assumption is about the three-dimensional wheel contact surface. The wheel circumferential profiles that are measured at different datum points on wheel tread are very similar as shown in Reference [1]. According to this, we assume that wheel circumferential profiles are the same no matter where measure datum points on transversal wheel tread are selected. In order words, the wear on the transverse profile is not considered. Hence the three-dimensional wear problem is simplified as a two-dimensional problem. In this paper, an averaged lateral position of contact patches on the wheel tread is used as the datum point to measure the profiles. It should be noted that in this paper 'profile' refers to the shape of the wheel out-of-roundness in circumferential direction instead of the wheel's transversal profile.

The general idea of simulating wear evolution is schematically illustrated in Figure 1 where the iterative calculation is divided into four basic parts. At the beginning, a profile of an initial polygonal irregularity that can be derived from the

manufacturing process, inhomogeneous materials or some other reasons is fed in a short-term vehicle dynamics model whose outputs in terms of creepages and creep forces are used by a wheel wear model to obtain a distribution of wear depth along the wheel circumference. This curve is processed by fitting methods to make it smooth and differentiable and is then subtracted from the circumferential profile of the wheel, resulting in an updated wheel profile which is fed back in the short-term vehicle dynamics model, so that the next calculation of material removal can be started. The procedure is iterated several times, providing the evolution of the wheel profile with cumulated service.

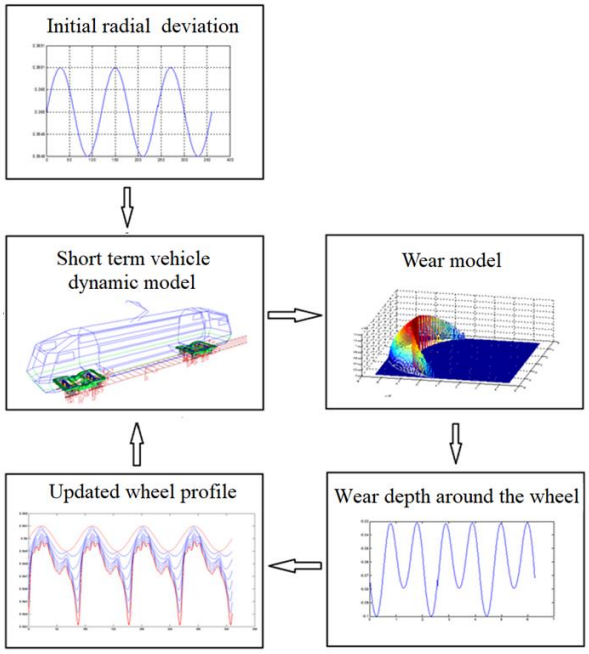

Figure 1 *Schematic simulation flowchart*

2.2. Wheel wear model

The wear of wheel tread in transversal direction has been studied for a long time and several wear models have been fully studied[12-14]. These models include, among others, the Archard model and the wear law based on frictional power. Since the wear mechanism taking place in the contact patch is identical for transversal and circumferential wear, it is natural to apply the same wear models to study polygonal wear.

Archard model, as a classical material wear model, has been widely used in railway engineering to predict wear at the wheel/rail interface. It is based on the following expression:

$$V_{wear} = k_w \frac{Nd}{H} \tag{1}$$

where V_{wear} is the volume of abraded material; N is the normal force applied on the surface; d is the sliding distance between two surfaces; H is the material hardness, and k_w is a wear proportionality coefficient. This model was implemented in the two recent studies for the polygonal wear simulation [15,16].

The wear model based on frictional power between wheel and rail has also been applied to study polygonal wheel wear [3,11,17,18,19]. This model assumes the excavated mass Δm is proportional to the wear energy W_R dissipated at wheel/rail contact due to friction. Equation (2) gives the basic calculation principle:

$$\Delta m = k(P_{RA}) \cdot W_R \tag{2}$$

where k is a proportionality factor depending on P_{RA} $[\mathrm{W}/m^2]$ which is the wear energy at unit contact area [3]. The wear

energy W_R is the product of integration step Δt *and* frictional power P_R which has three components in longitudinal, lateral and spin directions as is shown in Equation (3).

$$W_R = \Delta t \cdot P_R = \Delta t \, |T_x v_{rel,x} + T_y v_{rel,y} + M_\zeta \varphi_{rel,\zeta}| \quad (3)$$

$T_x v_{rel,x}$ *and* $T_y v_{rel,y}$ are products of creepage forces and relative velocities between wheel and rail in longitudinal and lateral directions. $M_\zeta \varphi_{rel,\zeta}$ is the product of the spin moment and relative rotational velocity between wheel and rail. The relative velocities between wheel and rail here are calculated as the product of corresponding creepages and vehicle speed. Equation (4) provides the method for computing the wear depth Δr at each contact patch:

$$\Delta r = \frac{\Delta m}{\rho A} = \frac{k|T_x v_{rel,x} + T_y v_{rel,y} + M_\zeta \varphi_{rel,\zeta}|\Delta t}{\rho A} \quad (4)$$

where ρ is the density of wheel material and A is the area of the contact patch.

It is worth mentioning that this wear model does not consider the local distribution of stresses and creepages inside the contact patch as is done in the "local wear" model described in the reference [20]. By contrast, in this "global wear" model, a mean value of the wear depth over the entire contact area is obtained from "global" quantities such as the creepages and creep forces. In reference [20] "local wear" and "global wear" models are compared and a good agreement is found, resulting in a maximum 4% difference between them. Because of the small difference of results provided by the two models, the approach of using a "global wear" model is adopted in this work as it enables a drastic reduction of the calculation time, given that it is not required to perform a local contact analysis to derive the distribution of stresses and slip in the contact patch. To summarize, in this work, the FASTSIM algorithm is used as the method to compute wheel-rail contact outputs and Equation (4) is implemented as the wear model.

2.3. Smoothing of the wear depth curve

The original curve of excavated material obtained from the short-term simulation of the vehicle dynamics model has spikes because of the rectangular element on the contact patch introduced from wheel-rail contact calculation and discretised distribution of contact patches around the wheel circumference. Smoothing is therefore required before wheel profiles are updated. Differently from the case of analysing the formation of tread wear, when polygonal wear is studied ,it has to be considered that the wheel circumferential profile is a closed line. The comparison of the two cases can be seen in Figure 2. Many traditional curve fitting methods like cubic interpolation and polynomial fitting cannot smooth a closed profile whilst ensuring that the curves are continuous and differentiable over the entire circumference. Continuity and differentiability are actual features of wheel profiles and are required in the simulation of wear formation since even a small discontinuity at the point connecting two ends of the curve will lead to impacts and result in wrong estimation of the polygonal wear pattern.

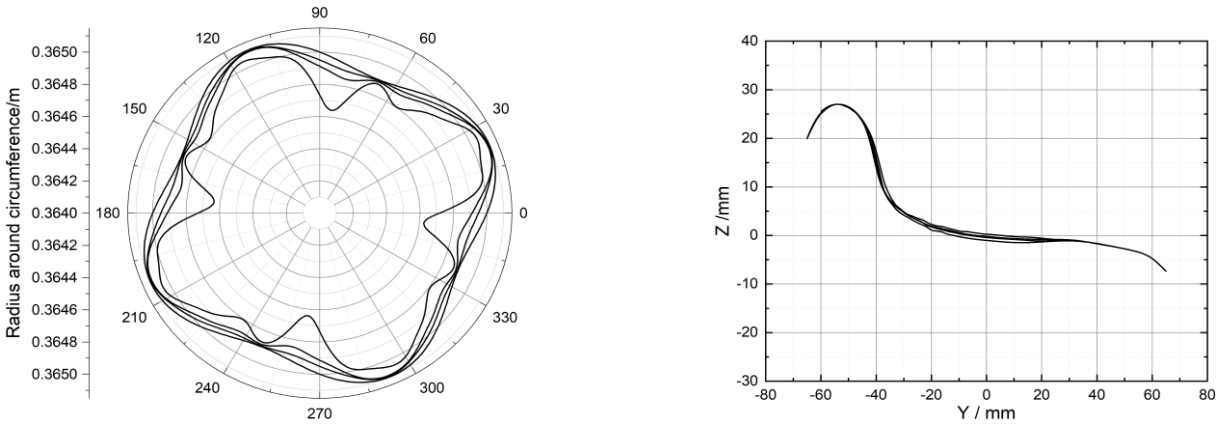

(a) *(b)*

Figure 2 *Comparison between (a) Closed wheel profile in circumference direction and (b) Unclosed wheel tread profile in transversal direction*

In this work, a fitting method based on Fourier Series is introduced to solve the problem. Equation (5) presents the truncated Fourier expansion used for curve fitting, where x and y are original data of wheel profile, and variables a_i and b_i are parameters to be identified. The linear combination of trigonometric functions can approximate any shape of wear curves if the number of harmonic terms considered is large enough. For a polygonal wear profile, the magnitude of the i^{th} polygon order is expressed by d_i defined according to Equation (6).

$$\begin{aligned} y(x) &= a_0 + a_1\cos(x) + a_2\cos(2x) + \cdots + a_n\cos(nx) \\ &\quad + b_1\sin(x) + b_2\sin(2x) + \cdots + b_n\sin(nx) \\ &= a_0 + \sum_{i=1}^{n}(a_i\cos ix + b_i\sin ix) \end{aligned} \tag{5}$$

$$d_i = \sqrt{a_i^2 + b_i^2} \tag{6}$$

Before applying Fourier series expansion function to fit the wear curve, the 'smoothing spline'[21] is applied to filter out the effect of numerical disturbances introduced by the short-term simulation. Figure 3 compares the original curve of excavated material, the curve filtered by the 'smoothing spline' and the Fourier series expansion function.

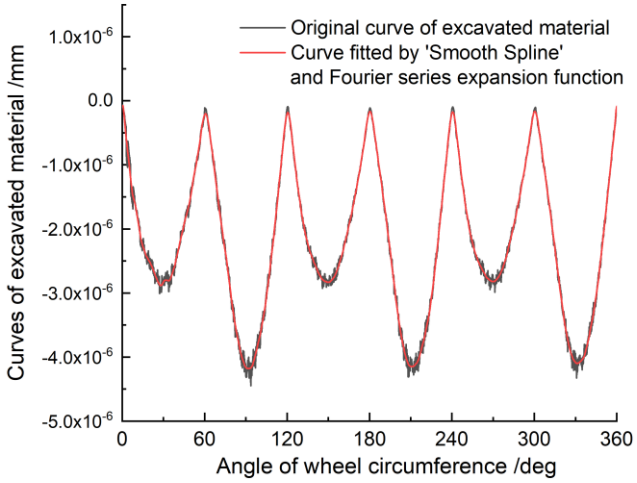

Figure 3 *Fitting effect for curves of excavated material*

2.4. Example of polygonal wear simulation

We built a dynamics model for a metro vehicle in SIMPACK where a sine function curve was applied to simulate the initial polygonal wheel irregularity. The number of wave crests around the wheel circumference equals to the wheel's polygon order and the amplitude of sine wave is the polygonal wear depth. In the simulation example, an initial wheel irregularity was configured as a 3rd order polygon with 0.1 mm depth. The evolution of wheel wear on a tangent track at speed 80km/h is shown in Cartesian coordinate and Polar coordinate in Figure 4 (a) and (b) respectively.

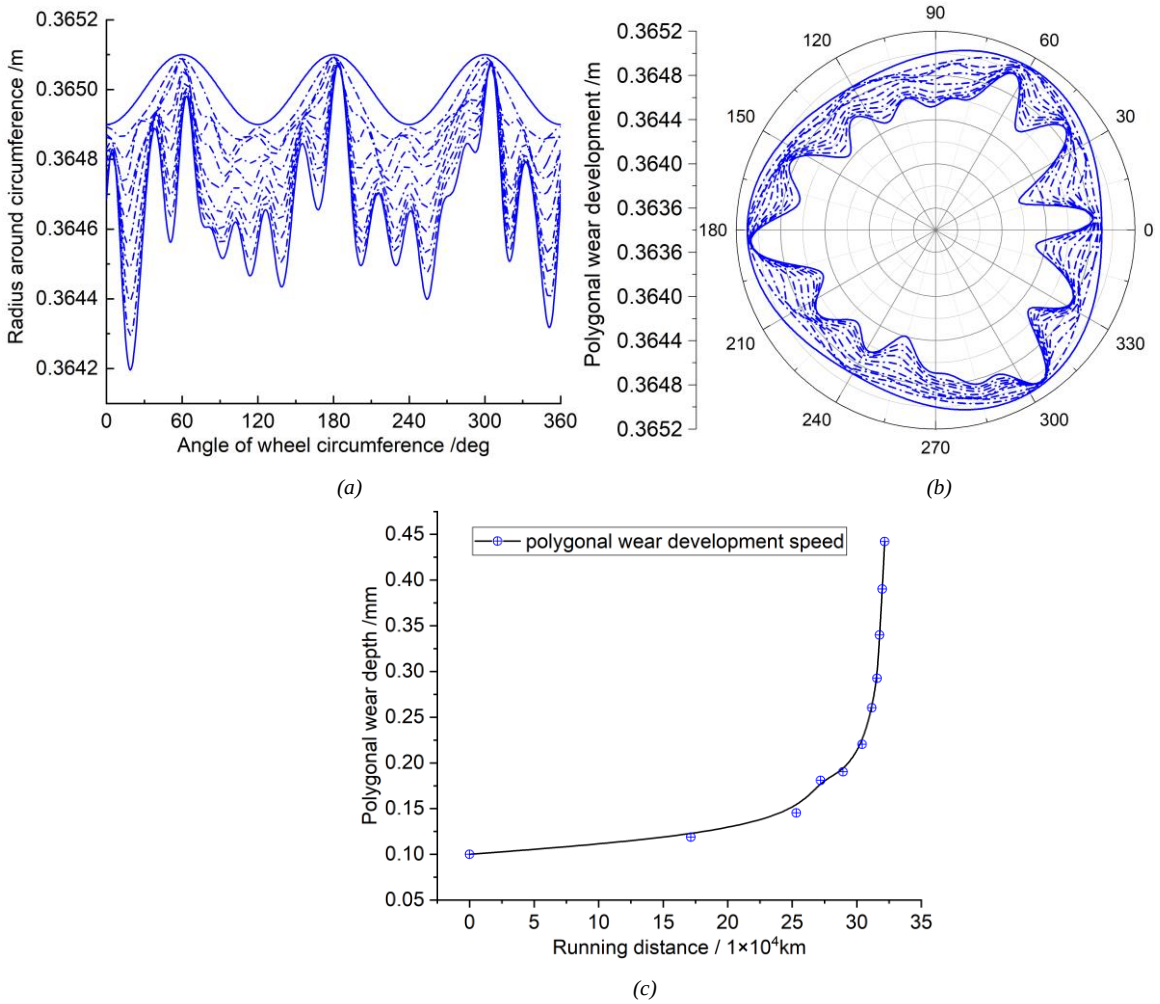

Figure 4 *Development of polygonal wear curves in (a) Cartesian coordinate, (b) Polar coordinate and (c) its polygonal wear depth over running distance*

With the progress of wear, the depth of the polygon increases, and new wave crests gradually appear. In order to explore the wear rate over the running distance, the simulated vehicle running distance is recorded before the wheel profiles are updated. The half of the distance from the absolute maximum to the absolute minimum value of the radius is defined as the polygonal wear depth. The wear rate is expressed as the gradient of polygonal wear depth vs. distance run, see Figure 4 (c). A scaling coefficient is applied to consider timescale effects in short-term simulation. This coefficient is estimated according to empirical observation on the polygonal wear. In this stage, it is impossible to get an accurate estimation for the scaling coefficient as detailed measurement data on wheel profiles are unavailable, but this only affects the total distance run by the vehicle to reach a given amplitude of irregularity, whilst it does not affect the evolution of the profile in terms of relative importance of the harmonic components of polygonization. Despite any possible uncertainty in the magnitude of the scaling coefficient, it is still meaningful to compare the relative growth rate of wear in different phases of the process. From Figure 4 (c), the slope of the curve illustrates that the growth rate increases with rising polygonal wear depth.

The development of polygon order in Figure 4 can be briefly explained by the phase difference between the time history of wheel circumferential profile and wheel-rail contact parameters as obtained from the short-term simulation. The time histories of wheel rolling radius, frictional power, wheel-rail normal force and vertical acceleration of linear motor are compared in Figure 5 (a). The frictional power directly reflects the location and amount of wear produced on the wheel. By comparing the values of three components of frictional power according to Equation (3), the lateral creepage dominates the contribution to the frictional power. The product of lateral creepage force and lateral relative velocity

between wheel and rail (i.e. $T_y v_{ref,y}$) has the same variation frequency as the radius curve. However, for the frictional power curve, the wave crests are doubled of wheel radius curve as the positive and negative peak values of $T_y v_{ref,y}$ form the two crests in each cycle. The normal force between the wheel and rail affects the size of contact patch area and also the amplitude of frictional power. The normal force changes according to the variation of wheel radius and also the vibration of its connected components. In this simulation model, the vibration of the linear motor significantly affects the normal force, as shown in Figure 5(a), where the normal force fluctuates according to the vertical acceleration of the linear motor.

The phase difference between the frictional power curve and wheel radius curve is essential to the development of polygonal wear. In our work, the variation of the phase difference is found at different speeds with different polygon orders, as shown in Figure 22 and Figure 23. In Reference [3], this varied phase difference was also observed and analyzed with a rigid and flexible track. The track property has an effect on the phase shift, but this phenomenon was not fully explained and cannot be precisely predicted. It should be noted that in our work, the vibrations of track components are not considered.

Four typical points are labelled in Figure 5 (a) and (b) to illustrate the change of polygon order. At time ①, wheel radius is at wave trough where the frictional power takes the lowest value, so the material loss in position ① is smaller than other positions. As a result, a new crest is formed in the updated profile as shown in Figure 5 (b). For time point ③, an original crest on wheel radius curve remains as less wear takes place. At time ② and time ④, the frictional power reaches peak values, so the amount of removed materials is larger than those of the positions around and hence two troughs are formed.

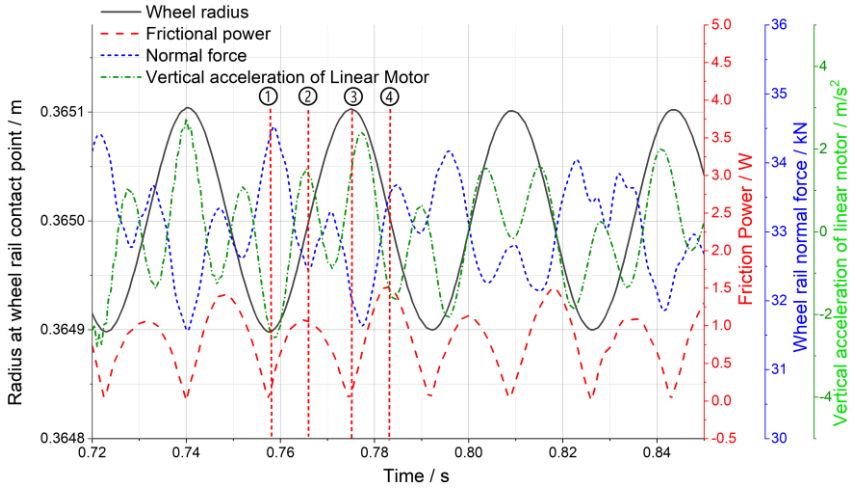

(a)

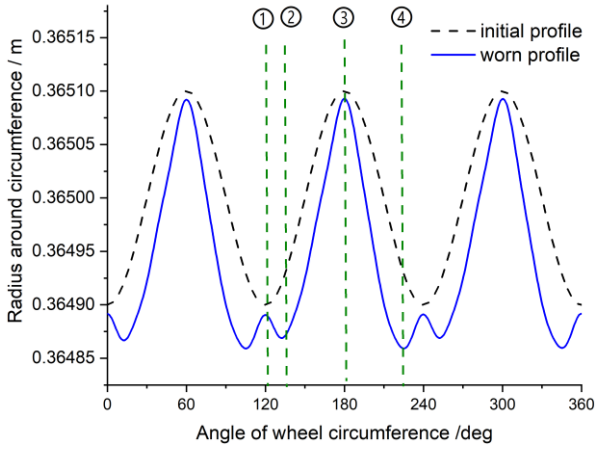

(b)

Figure 5 *Investigation for increase of polygon order: (a) Time histories of wheel radius, frictional power, normal force and vertical acceleration of linear motor and (b) Initial profile and worn profile after the first iteration*

3. Effects of simulation parameter settings and calculation error analyses

Even though the simulation approach for polygonal wear evolution has been introduced in the section above, some parameter settings can change the simulation results and because of considerable errors. In order to improve the reliability of the model, we studied three key settings: time step used for numerical integration, curve fitting method and wheel profile updating strategy.

3.1. Time step for numerical integration

The size and number of time-integration steps influence the simulation accuracy. If a large step size and a small number of integration steps are set, the contact patches calculated around the wheel will not be fully overlapped. It causes disturbance on material excavation curve, resulting in short-wavelength components of the out-of-roundness that are of artificial nature. The original excavated material curve in a single short-term simulation with different simulation time and numbers of integration steps are shown in Figure 6. The disturbance will be effectively eliminated when the number of steps is greater than 10000. We don't give a general standard for integration number, because the disturbance could be larger if a higher order wear curve appears in the subsequent iterations. To ensure the calculation accuracy, the number of integration steps for the following simulations in this paper is greater than 20000.

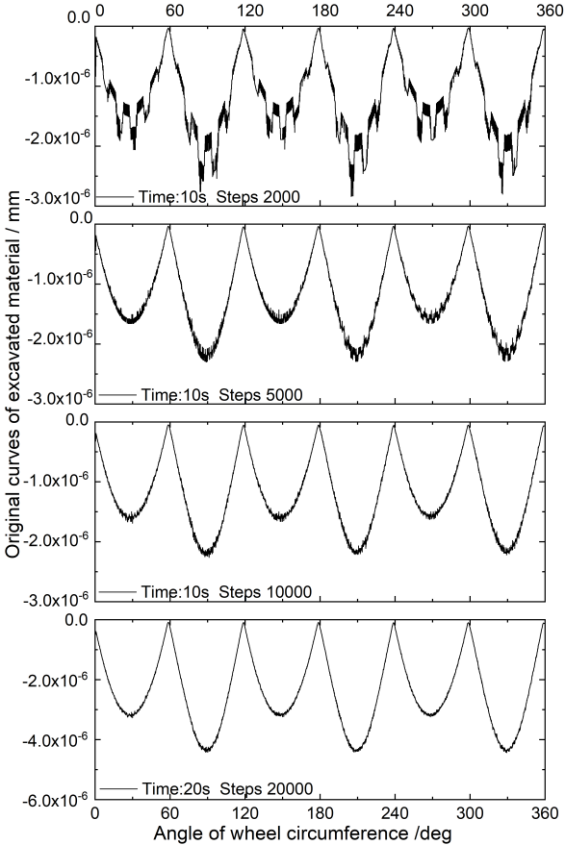

Figure 6 *Original curves of excavated material with different calculation steps*

3.2. Curve fitting methods

The second error of wear calculation comes from curve fitting methods. As is described in Section 2.3, a smoothing spline followed by a truncated Fourier series expansion of the wear depth function is performed to eliminate discontinuities

arising from the short-term simulation process. The parameter settings adopted in the two smoothing methods have an influence on the smoothed wear depth profiles.

For the smoothing spline, it is not difficult to set a suitable 'Smoothness' to recognize real polygonal wear curve from disturbance when the number of numerical integration steps is large enough and the order of polygon is not so high, but in adverse cases, the error cannot be fully avoided.

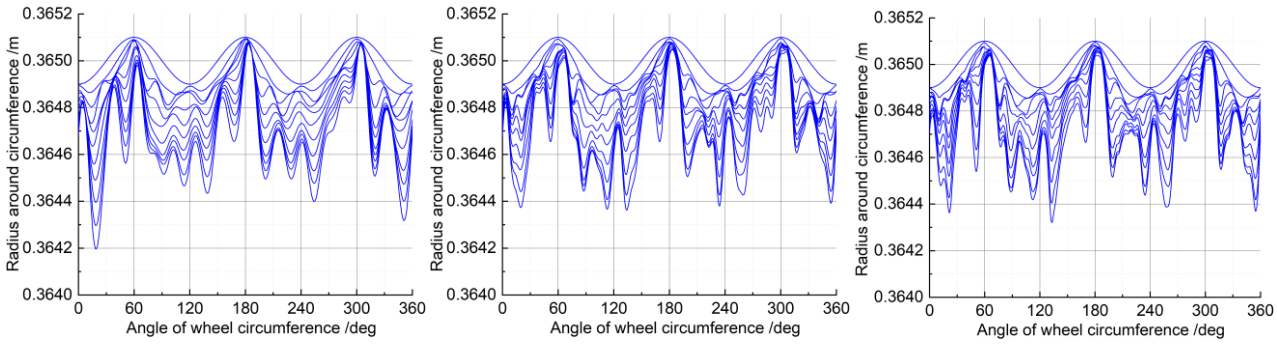

(a) n =20 *(b) n =40* *(c) n =100*

Figure7 *Polygonal wear curves at simulation speed 80km/h, with different harmonic function number n: (a)n=20, (b)n=40 and (c) n =100*

As far as the truncated Fourier series expansion is concerned, the number of harmonics *n* (see Equation 5) determines the level of detail to which the input profile is approximated. Theoretically, *n* should be selected as large as possible to reduce the curve fitting error and *n* is also the upper limit for the maximum orders that the simulation model can analyse. However, numerical disturbances not sufficiently filtered by the smoothing spline could be retained and would then affect the next iteration of the calculation, see Figure 1. Hence, it could be advisable to apply a relatively small *n* when low order polygons are studied. Figure 7 shows wear development curves when *n* is configured to 20, 40 and 100 respectively. The main evolution features are similar, but the wear profiles additionally show some short-wavelength fluctuations when *n* is equal to 100. In the following simulations in this paper, *n* is configured to 100.

3.3. Wear profile updating strategy

The criterion for updating the wheel profile is another important setting in the long-term wear model. In this work, a constant depth ΔD is used to control the maximum wear depth between successive profile updates. Figure 8 compares the results of polygonal wear of a metro wheel with an initial triangle irregularity at 50km/h for depth ΔD varying from 0.2mm to 0.05mm.

A simulation with too large ΔD may lead to a divergence of the simulated wear process from the real one. However, too small depth ΔD means a large number of iterations in the iterative process illustrated by Figure 1 and hence entails a more intensive use of computing resources. Furthermore, when too many iterations are applied a small error, arising for instance from curve fitting methods, could be gradually magnified. Hence too small ΔD should also be avoided. The comparison of Figures 8 (a), (b) and (c) shows a converging trend in the shape of the polygonal profile with reducing the ΔD parameter. Despite a difference between Figure 8 (b) and (c) is still visible, wear patterns in these two plots are quite similar. We ,therefore, consider ΔD=0.1mm as the standard depth value to be used for profile updating in our work. But it is noted that when wear evolution starts from an initial profile for which the polygon depth is lower than 0.1mm, a smaller ΔD would be recommended.

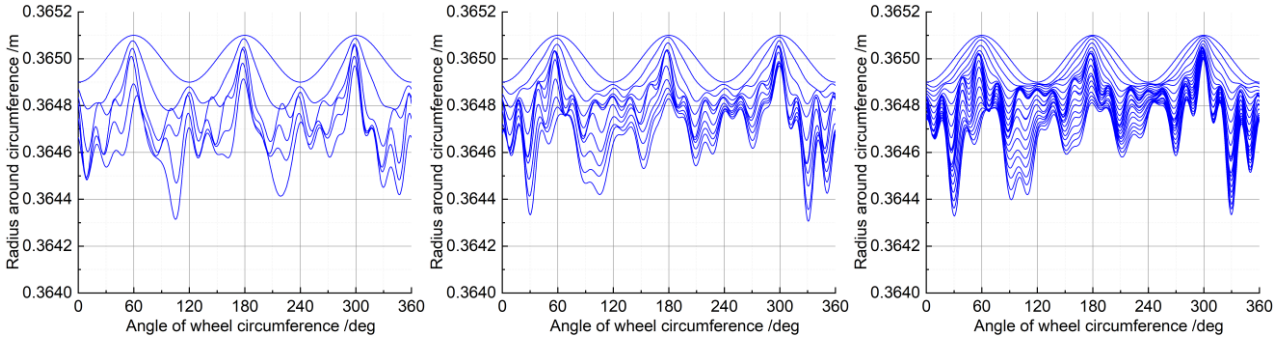

(a) ΔD=0.2mm *(b) ΔD=0.1mm* *(c) ΔD=0.05*mm

Figure 8 *Polygonal wear curves at simulation speed 50km/h with different profile update depth ΔD: (a) ΔD=0.2mm, (b) ΔD=0.1mm and (c) ΔD=0.05*mm

4. Case study: wheel polygonization of a metro vehicle

4.1. Brief introduction of the metro vehicle and its dynamics model

A metro vehicle with the linear motor traction technology is found to have mainly 8th to 9th orders polygonal wheel when running several months after wheel re-profiling, leading to poor ride comfort. A unique feature of this bogie architecture is the linear motor which is connected to the bogie frame in lateral and longitudinal directions by several rods with elastic bushings. In the vertical direction, five rods attach the linear motor on two beams which are mounted on axle-boxes through stiff bush components [22]. Figure 9 presents the suspension structure of the linear motor. The wheels have an initial 4th order polygon after re-profiling. This initial out of roundness originates from the technology adopted for wheel re-profiling where geometric eccentricity of wheel centre cannot be completely avoided in the turning process [23]. Simulation work and long-term field tests were carried out to investigate this problem.

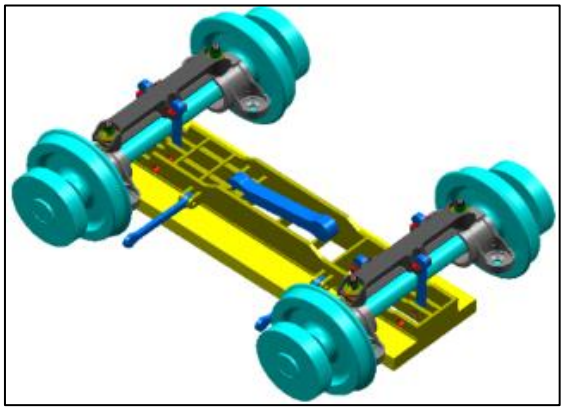

Figure 9 *Suspension structure of the linear motor*

The vehicle dynamics model was built in software SIMPACK. This model considers the flexibility of the wheelset by means of a modal synthesis derived from a finite element model of an unconstrained wheelset. The finite element model of the wheelset and mode extraction was performed in ANSYS, showing that the frequencies of the first torsion mode, the first bending mode and the second bending mode are 78.0Hz，83.0Hz and 195.9Hz respectively. Figure 10 displays the shape of the first bending mode.

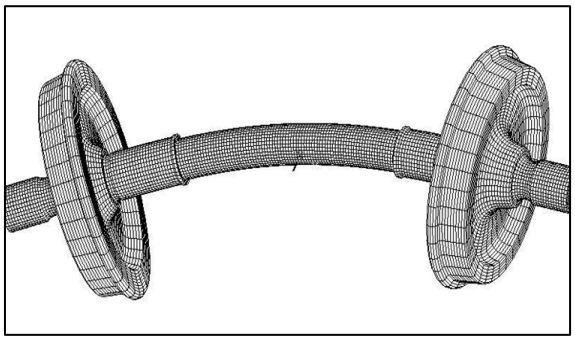

Figure 10. Shape of the first bending mode

Track flexibility also affects wheel/rail contact forces at relatively high frequencies with possible effects also on polygonal wear. However, considering the additional complexity entailed by a model considering track flexibility and especially the lack of experimental data regarding the track system, in this work the track is considered as a fixed system.

For this metro vehicle, the frequency range of excitation caused by 8^{th} to 9^{th} order polygonal wheel in normal running speeds (20-90km/h) is 22-98 Hz approximately. The rigid mode frequencies of the vehicle model were calculated in SIMPACK and all the interested vehicle vibration modes are listed in Table 1.

Table 1 Vibration modes and their natural frequencies

Vibration modes	Natural frequency
Bogie frame rolling	11.1Hz
Bogie frame bouncing	22.0Hz
Bogie frame yawing	32.5Hz
Bogie frame lateral oscillation	33.2Hz
Linear motor bouncing	41.7Hz
Linear motor pitching	58.3 Hz
Linear motor rolling	78.5Hz
Wheelset first torsion mode	78.0
Wheelset first bending mode	83.0
Wheelset second bending mode	195.9

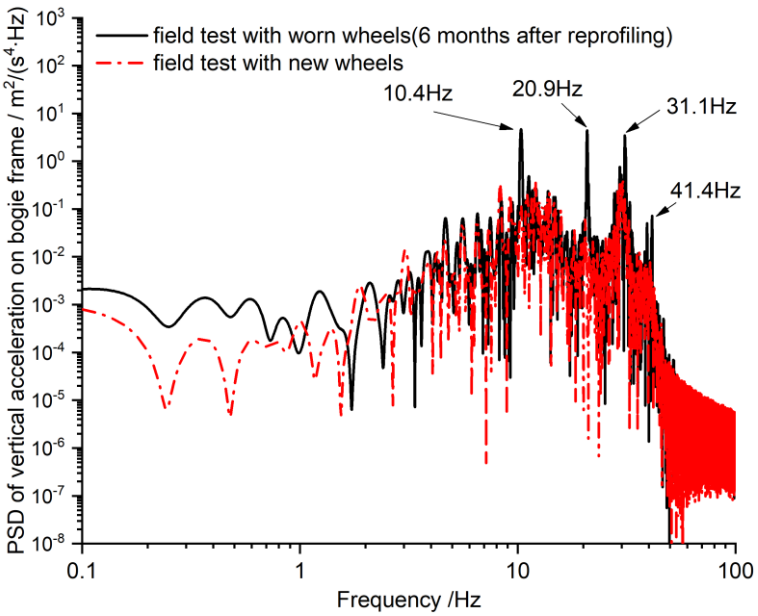

Figure 11. PSD analysis of vertical acceleration measured on the bogie frame ·

The vehicle on-track tests were carried out with new re-profiled wheels and worn wheels 6 months after reprofiling. Accelerations were measured on the car-body and on the bogie frame. The 20-second acceleration on the bogie frame is analysed when the vehicle speed kept at around 80-85km/h. Figure 11 shows the PSD (Power Spectral Density) of the vertical acceleration on the bogie frame. The comparison of the measured bogie acceleration in the two tests with new and worn wheels illustrates that with the progress of wheel wear, bogie vibration becomes more intense. Four peaks are observed in the measurement performed with worn wheels. The peaks are at 10.4Hz, 20.9Hz, 31.1Hz and 41.4Hz which are in line with the natural frequencies corresponding to frame rolling, frame bouncing, frame yawing and linear motor bouncing as shown in Tab. 1. Since the vibration of the linear motor is attenuated by the primary suspension (vertical stiffness: 1.2MN/m per axle-box), the peak at 41.4Hz is not as high as the other ones which are related to bogie frame vibration. The small discrepancies between the measured and calculated frequencies could come from errors in model parameters, such as stiffness of springs and mass of the frame.

4.2. Dynamic performance of the vehicle and resonance speed identification

As poor ride comfort is one main issue of concern, we assessed the lateral and vertical ride comfort through Sperling ride index Wz. This factor is calculated in the SIMPACK built-in Post-Processing Program where the standard algorithm considers the frequency weighting functions defined in ISO 2631[24] to reflect the effects of vibrations at different frequency range on the ride comfort. The values of index Wz should be lower than 3 which represents the "tolerable level" for the ride comfort and in the metro company they use the value 2.5 as a criterion for "excellent level". The verbal description of different values of Wz and further explanation can be found in Reference [25].

The simulations were performed to analyse the ride index of the vehicle travelling at different speeds with 8th and 9th order polygonal wheels as shown in Figure 12 and Figure 13.

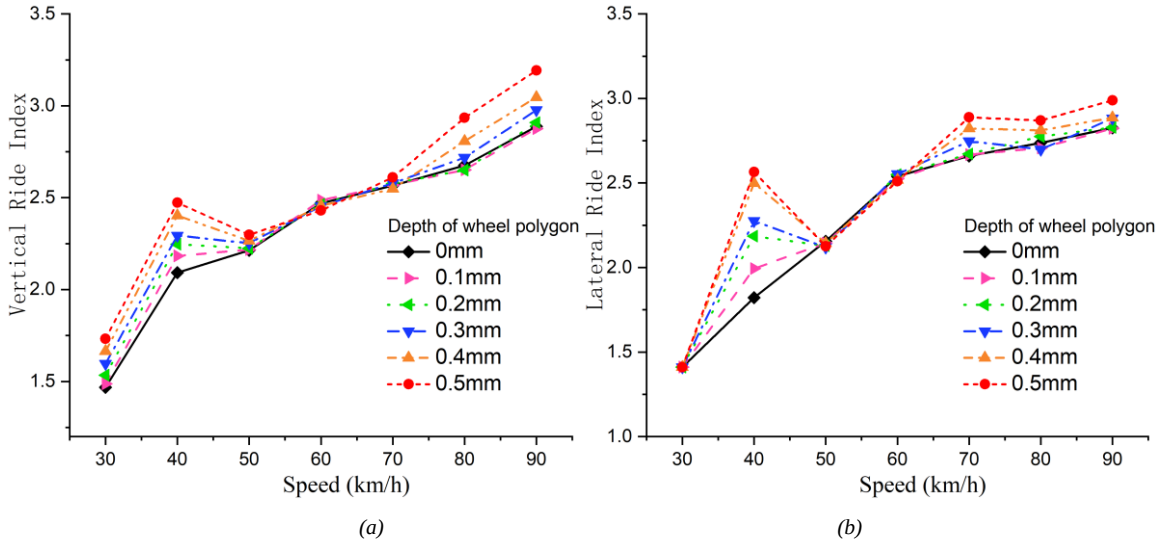

Figure 12 *Sperling ride index of the vehicle with 8th order polygonal wheel at different speeds in (a) vertical direction and (b) lateral direction*

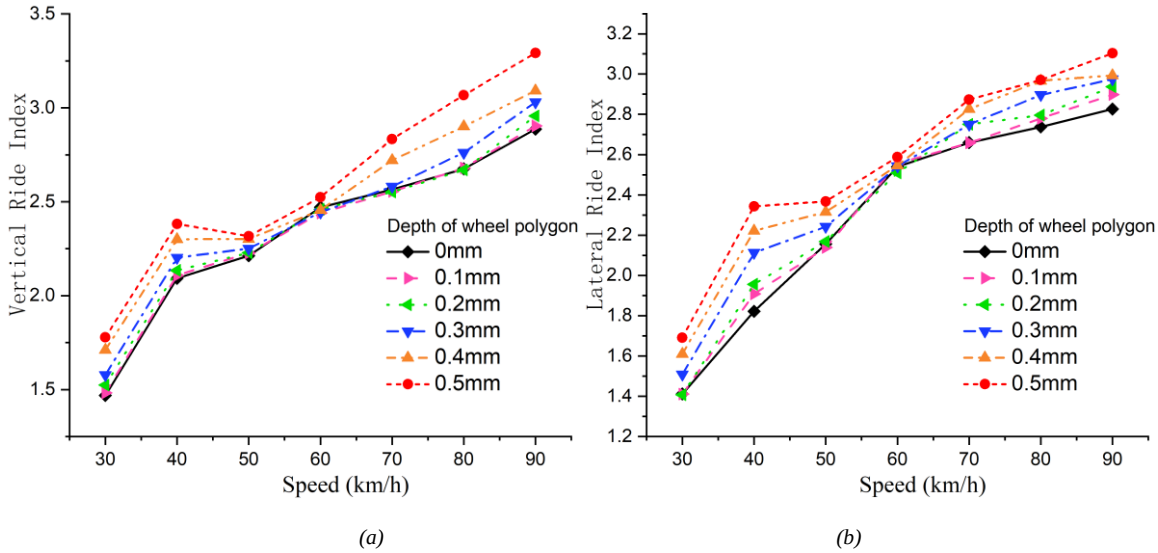

Figure 13 *Sperling ride index of the vehicle with 9th order polygonal wheel at different speeds in (a) vertical direction and (b) lateral direction*

The ride indexes in both lateral and vertical directions show particularly large values when the vehicle speeds are close to 40km/h, and these peak points become higher with the increase of polygonal wear depth. This peculiar phenomenon suggests that a resonance phenomenon occurs at this speed. Indeed, when the vehicle speed is 40km/h, the 8th and 9th order harmonics of wheel polygonization produce a forcing effect at 38.8Hz and 43.6Hz respectively, which are close to the natural frequency of the linear motor's bouncing motion, 41.7Hz. Therefore, the motor resonance is excited, resulting in significant degradation of both vertical and lateral ride indexes.

A series of long-term field tests were carried out in the first month, the second month and the sixth month after wheel re-profiling. The vehicle was tested on the main metro line in tare condition and was operated in the driverless mode which is the normal way in standard service. Because of this, the time histories of the vehicle speed between any two stops are the same in all tests, so the accelerations measured at the same location in different tests can be thoroughly compared. In this paper, measured data on a typical straight track zone between two adjacent stations is used for analysis where the vehicle accelerates to 85km/h and then decelerates to zero within around 90 seconds. The vertical and lateral ride indexes are processed over records of car body acceleration having a duration of 5 s each and the results of this analyses are presented in Figure 14 and Figure 15.

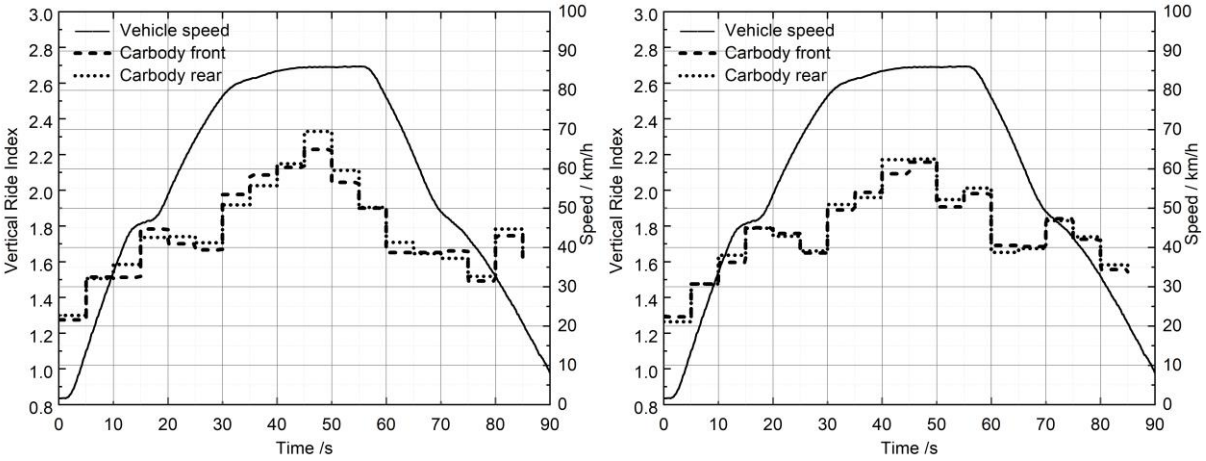

(a) *1 month after wheel re-profiling*

(b) *2 months after wheel re-profiling*

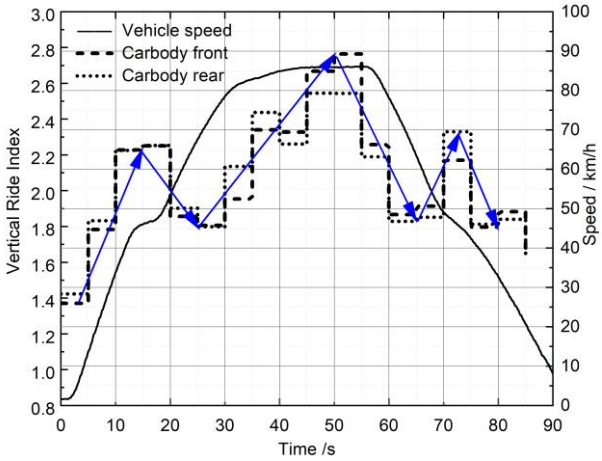

(c) *6 months after wheel re-profiling*

Figure 14 *Vertical ride index and speed time history curve measured between two metro stations*

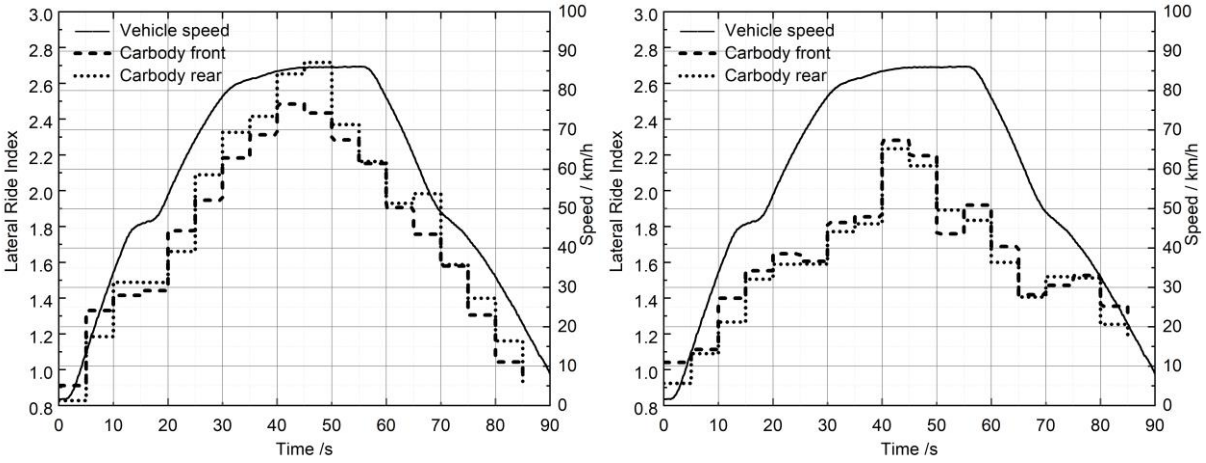

(a) *1 month after wheel re-profiling*

(b) *2 months after wheel re-profiling*

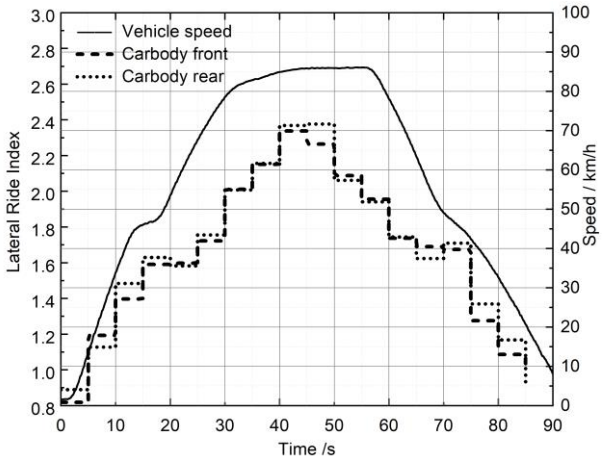

(c) *6 months after wheel re-profiling*

Figure 15 *Lateral ride index and speed time history curve measured between two metro stations*

Based on these figures, some features can be summarised as follows:

(a) When the vehicle travelled at a speed of approximately 40km/h during the acceleration and deceleration transients，the vertical ride index became very large and sometimes unacceptable, as pointed by the blue arrows in Figure 14 (c). This feature became more apparent in later months with the development of wheel polygonization.

(b) The vertical ride index over the whole track zone was relatively good after re-profiling, but became increasingly worse in later months.

(c) The lateral ride index was poor after wheel re-profiling, especially when running speed was close to 80-85km/h. However, in the following months, the ride index in the high-speed range was improved.

The above concluded three features were also observed in other test zones with a similar track layout and time history of vehicle speed. Namely, points (b) and (c) were noticed and claimed by the staff in the metro company even before the tests were carried out. As far as point (a) is concerned, it validates the simulation results in Figure 12 and Figure 13, confirming bad ride comfort at the speed of 40 km/h, and this is much likely related to the resonance of the linear motor. Evidences (b) and (c) require a more detailed discussion which is provided in Section 4.3.

4.3. Polygonal wear for the metro vehicle

Besides the resonance condition at speed close to 40km/h generated by 8^{th} and 9^{th} orders of wheel polygonization, a second critical speed is found at 85km/h that can cause resonance of the linear motor in presence of a 4^{th} order of wheel polygonization.

Figure 16 (a) presents a typical time history of speed from field tests in a straight zone. Although the vehicle travels at non-constant speeds, the discrete speed data in Figure 16 (b) shows that the most frequent running speed is around 85km/h. According to this analysis, polygonal wear development at speed 85km/h could be of great importance.

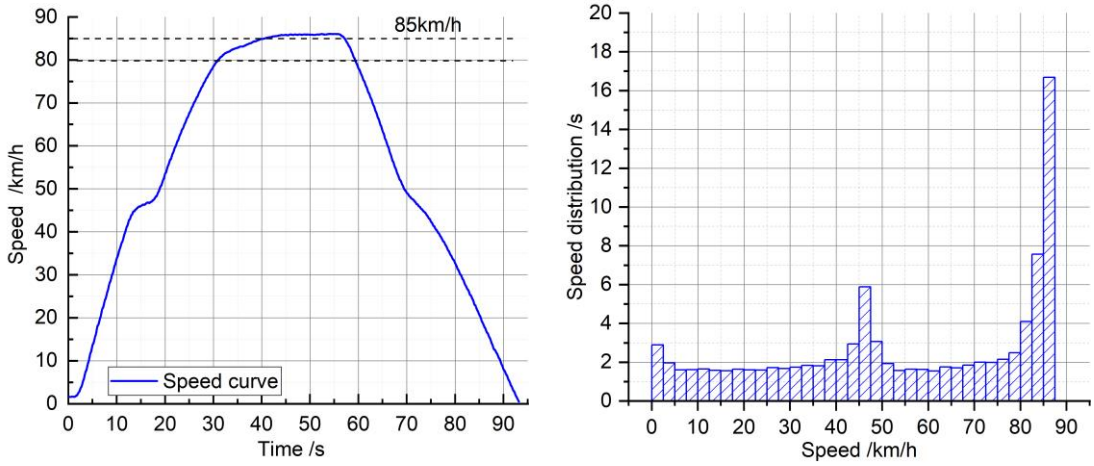

(a) *(b)*

Figure 16 (a) *Typical speed time history and (b) its speed distribution*

The development of polygonal wear for this running condition was simulated using the iterative wear model described in Section 2. An initial 4th order polygonal irregularity with a depth of 0.1mm arising from the wheel turning process is considered and parameter ΔD defining the profile updating criterion is set to 0.1mm. In Figure 17, the wheel profiles obtained in fifteen successive iterations of the simulation are shown to describe wear evolution at speed 85km/h.

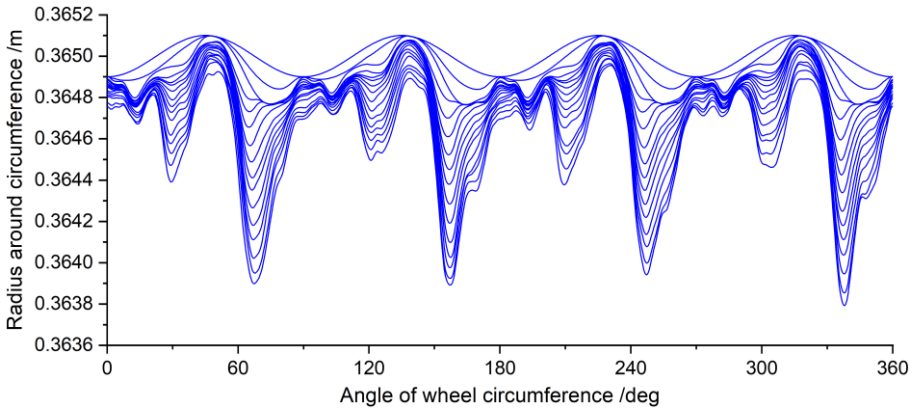

Figure 17 *Evolution of polygonal wear of the metro wheel at speed 85km/h; ΔD=0.1mm, harmonic order n=100*

From this representation, an increase of polygonal wear depth and the presence of higher orders of polygonization can be noticed, but the contributions of different orders to the wheel profile cannot be assessed on quantitative grounds. In order to quantify the components of different orders, the roughness level L_r^k is calculated according to Equation (7)

$$L_r^k = 20log10\frac{\widetilde{r_k}}{r_{ref}} \tag{7}$$

where $\widetilde{r_k}$ is the amplitude of different wavelengths in one-third octave band and the r_{ref} is the reference value of wheel roughness set to 1 μm[26,27]. Figure 18 shows the development of roughness levels for the first 30 polygon orders in the wear evolution with 15 iterations. Except for the initial fourth polygon order, the 7th to 9th order components show the largest amplitude, followed by the 11th to 13th order components.

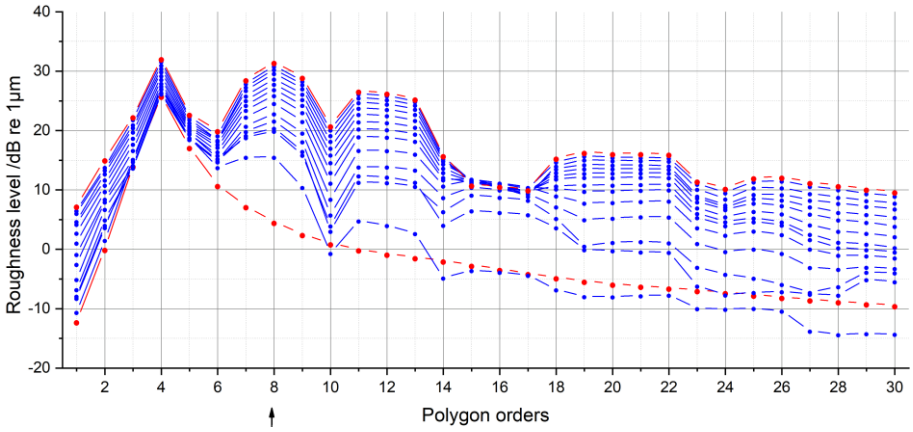

Figure 18. *Roughness level over the first 30th orders.*

In order to further investigate what happened in this wear evolution process, the frictional power is firstly analysed and a few of other simulations in different configurations are calculated for comparison. Six simulation configurations are designed and listed in Table.2.

Table.2 Simulation cases

Simulation cases	Configuration
Case 1	Vehicle speed: 85 km/h； Polygon order: 4th order
Case 2	Vehicle speed: 90 km/h； Polygon order: 4th order
Case 3	Vehicle speed: 70 km/h； Polygon order: 4th order
Case 4	Vehicle speed: 85 km/h； Polygon order: 3rd order
Case 5	Vehicle speed: 68 km/h； Polygon order: 5th order
Case 6	Vehicle speed: 85 km/h； Polygon order: 8th order

For the above-mentioned simulation scenarios, the time histories of wheel frictional power and the corresponding PSDs are presented in Figure 19 (a) and (b).

The amplitude of the frictional power in time domain reflects the intensity of the wear. In Case 1 (4th order, 85km/h), the wheel generates intensive wear, because the 4th order polygonal wheel produces excitation at around 41Hz and excites the resonance of the linear motor. For this case, in Figure 19 (b), the frequency component at 41 Hz is clearly noticed together with a double frequency vibration at around 82Hz. This component at double frequency mainly comes from the positive and negative peak values of $T_y v_{ref,y}$ in each vibration cycle, as was explained for Figure 5, in Section 2.4. The presence of a peak at double frequency of with respect to the main excitation is hence visible not only for case 1, but for all cases, as is pointed by the red arrows in Figure 19 (b).

Case 2 (4th order, 90km/h) and Case 3 (4th order, 70km/h) are characterised by the same initial wheel out of roundness, but vehicle speed is different so that the resonance effect arising at 85 km/h is much attenuated.

Case 4 (3rd order, 85km/h) also supports the conclusion that vehicle speed is not the dominating reason for severe polyonal wear. In order to ensure that the intensive wear is related to the vertical vibration of the linear motor, in Case 5, an initial out of roundness with a 5th order component is considered together with a vehicle speed of 68 km/h so that again the forcing frequency is set at 41Hz. The results show a level of frictional power very similar to the one shown in Case 1.

Altogether, Case 1 and Case 5 prove that a 41Hz excitation from the initial wheel out of roundness excites the resonance of the linear motor thus increasing wear drastically, but a significant component of frictional power is also found at 82 Hz, which is close to 83Hz, the frequency of the first bending mode of the flexible wheelset. Then, it becomes doubtful whether the severe wear comes from the vibration of the linear motor or the first bending mode of the wheelset.

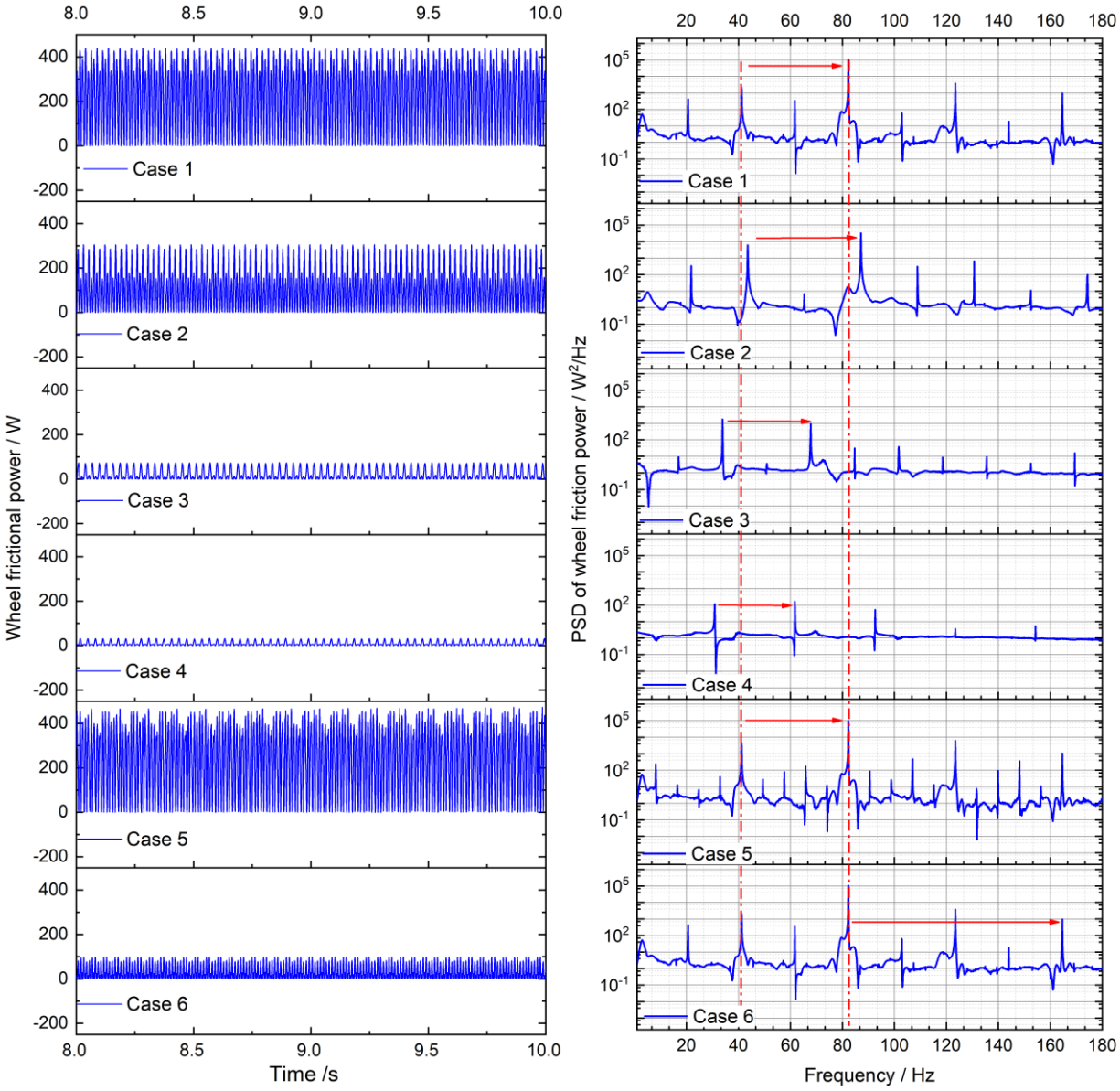

Figure 19. *(a) Time history of wheel frictional power and (b) PSD of wheel frictional power*

In Case 6, the vehicle speed is again 85km/h, but the polygon order is doubled from 4th to 8th order. By doing so, the wheel excitation shifts from 41 Hz to 82 Hz. This frequency is much higher than the resonance frequency of the linear motor and consequently the motor resonance will not be excited, but a more intense excitation is expected for the first bending mode of the wheelset. The PSD analyses of vertical and lateral accelerations on axle-box are displayed in Figure 20, comparing cases 1, 4, 5 and 6. Among all cases considered in this figure, Case 6 shows the highest value of vertical acceleration at around 82Hz, confirming intense excitation of the wheelset first bending mode for this case. Nevertheless, in Figure 19 (a), the frictional power in Case 6 is still much less than the ones in Case 1 and Case 5. The frictional power is mainly contributed by the lateral slip and Figure 20 (b) shows that the maximum lateral acceleration at 82 Hz is still

obtained in Case 1 and Case 5 where the resonance of the linear motor takes place, in agreement with the results shown in Figure 19. In conclusion, despite the first bending mode of the wheelset can be excited through a proper combination of the initial wheel out of roundness and vehicle speed, it is confirmed that the resonance of the linear motor is the dominating factor for the drastic increase of the polygonal wear.

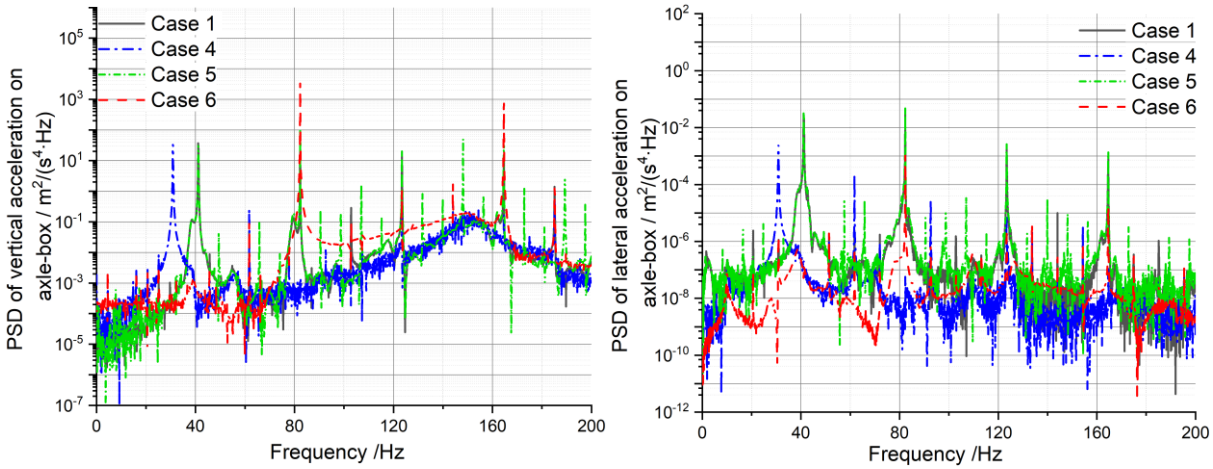

(a) (b)

Figure 20 *PSDs of (a) Vertical acceleration on the axle-box and (b) Lateral acceleration on the axle-box*

The analyses above studied polygonal wear evolution started from the initial 4th order polygon. In this part, a wear simulation focuses on the phase after the 8th order polygonal wheel is formed. A new wear evolution is simulated with an initial 8th order polygon, at speed 85km/h, the same as the configuration in Case 6. The wear evolution in Figure 21 clearly shows the increase of polygonal wear depth but no change of polygon order, differently from the wear pattern arising from an initial 4th order polygonal wheel as shown in Figure 17.

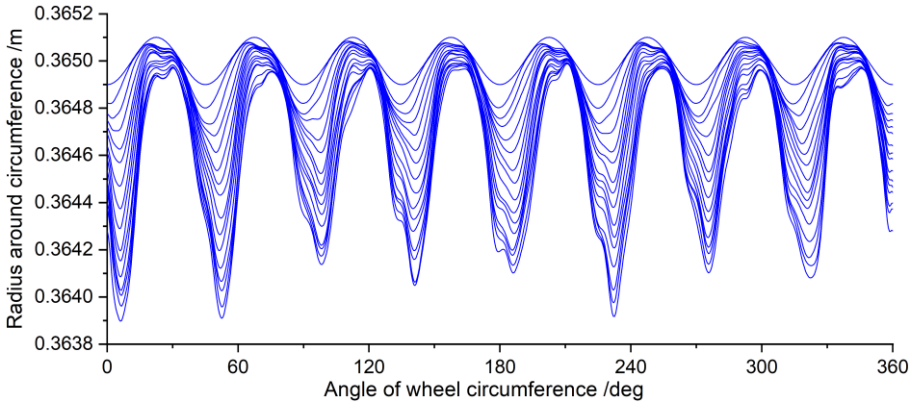

Figure 21 *Evolution of polygonal wear started from 8th polygon, at speed 85km/h; ΔD=0.1mm, harmonic order n=100*

In order to investigate the difference between the two wear patterns, the time histories of the wheel radius, frictional power, wheel-rail normal force and vertical acceleration of the linear motor in two cases are presented in Figure 22(a) and (b). In Case 1, with the initial 4th order polygon, the maximum frictional power takes place in the centre between the crest and trough of wheel radius curve and the minimum power occurs at the crest and trough of the radius curve. This feature is similar to that of Figure 5(a) and the worn profile performed after the first iteration in Figure 23(a) looks like Figure 5(b). By contrast, with an initial 8th order polygon, the maximum frictional power appears at the trough of wheel radius curve. In these positions, much material is removed, resulting in the increase of polygon depth, as shown in Figure 23(b). In case 6, the lateral slip is reduced as you can see that the amplitude of frictional power in Figure 22(b) is smaller than that in Figure 22(a). In Figure 22(b), the second maximum power is much lower than the first one because a smaller normal force in the corresponding position reduces the interaction forces between wheel and rail. The variation of the

normal force is caused by the shape of the wheel and also the vibration of the linear motor. These parameters interact with each other in a complicated way and result in the phase shift between the wheel radius and frictional power which principally decides the evolution of the polygon order.

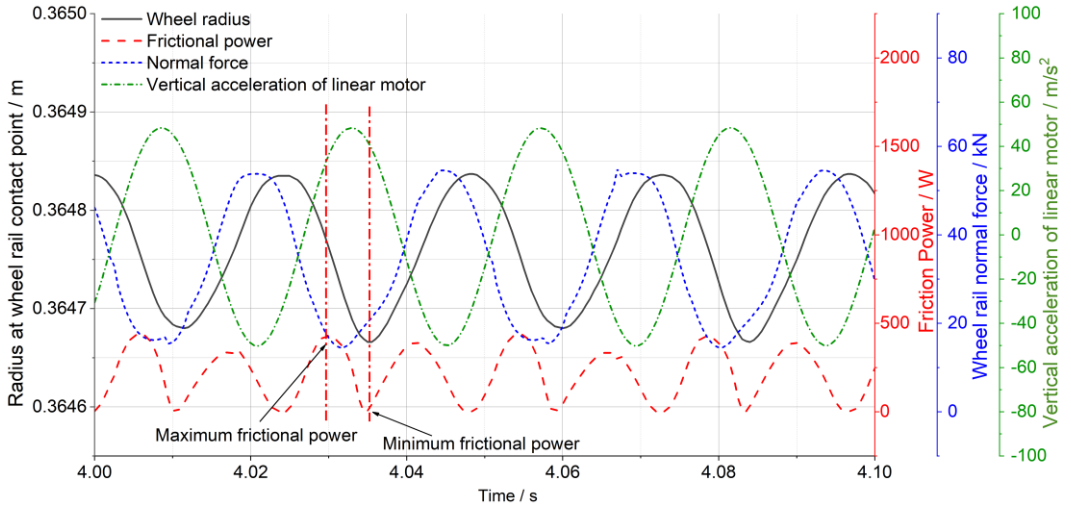

(a) Case 1 (initial order:4th order; speed: 85km/h)

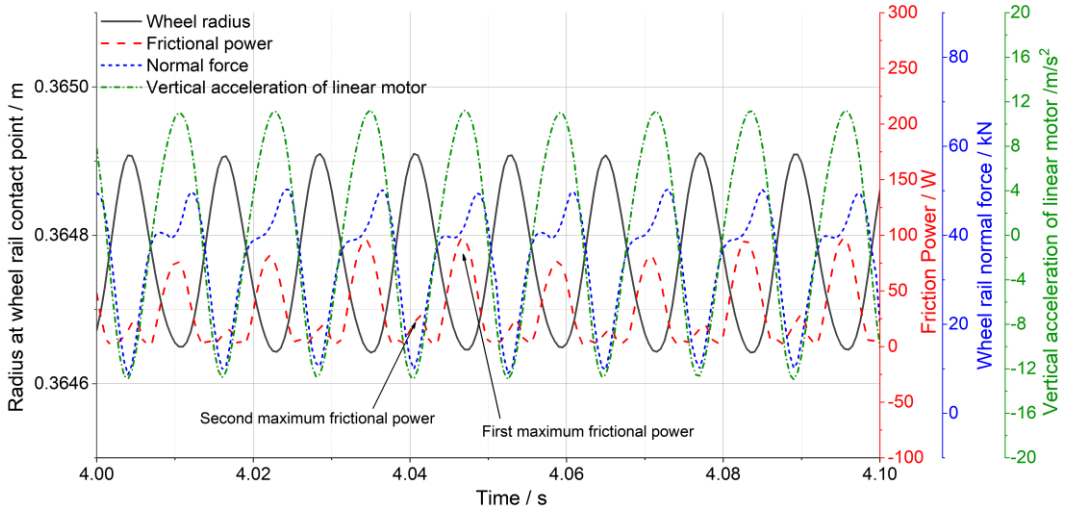

(b) Case 6 (initial order:8th order; speed: 85km/h)

Figure. 22 *Time histories of wheel radius, frictional power, wheel rail normal force and vertical acceleration of the linear motor for (a) simulation Case 1 and (b) simulation Case 6*

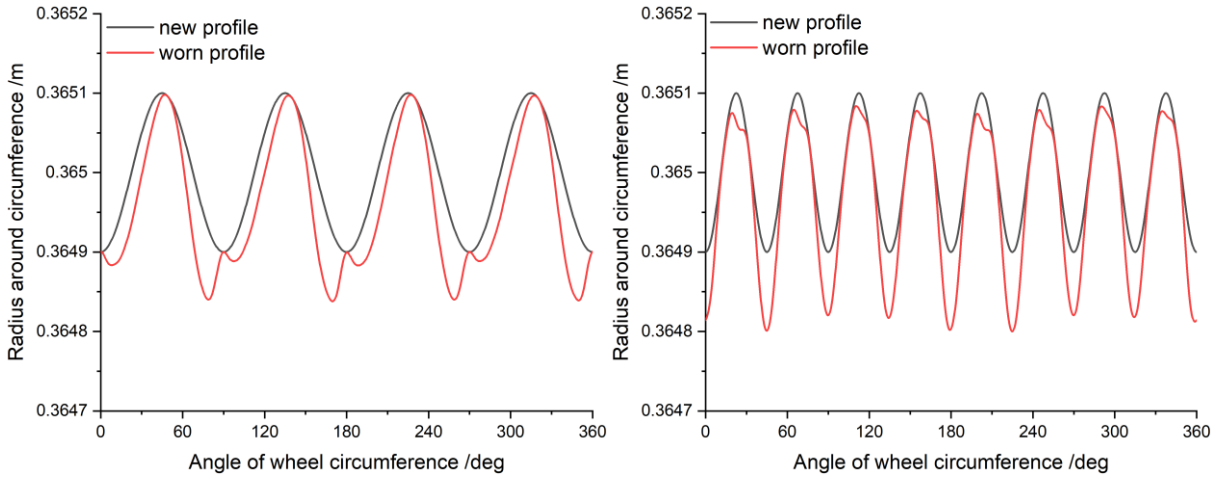

(a) Case 1 *(b) Case 6*

Figure 23 *Worn profile after the first iteration of wear evolution with (a) the initial 4th order (Case 1) and (b) the initial 8th order (Case 6)*

Based on these wear simulations and field tests, the following mechanism is proposed to explain the formation of the polygonal wear starting from an initial 4th order polygon and finally resulting in the 8th and 9th order polygonization.

In the initial phase, with the 4th order polygonal irregularity, the wheels will produce around 41Hz excitation at speed 85km/h, which causes the resonance of the linear motor. The vibrations of the car-body, linear motor and wheelset in this situation become severe. According to the speed distribution, keeping the running speed at 85km/h for a long time accelerates the polygonal wear development from the initial 4th order into the 8th and 9th order.

When the 8th and 9th order polygonal wheels appear, the wear enters into the second phase, in which the new order polygonal wheel at 85km/h produces frequency higher than 80Hz. Hence it will no longer cause the resonance of the linear motor. In this stage, the order of polygon will not change dramatically, but the depth of polygonal wear will continue increasing.

This mechanism is in accordance with some peculiar phenomena observed in field tests, which have been introduced in Section 4.2, see particularly points (a) to (c). For point (b), the deterioration of vertical ride index from the first month to the sixth month, came from the increase of polygonal wear depth in both phases, especially in the second phase after the 8th and 9th order polygon was formed. For point (c), the improvement of lateral ride index at maximum speed 85km/h observed in the next months, could be due to the fact that after the initial 4th order polygonization is transformed in the 8th and 9th polygonization the resonance of the motor is no longer excited at 85 km/h. Instead, a different resonance speed at around 40km/h was observed, which is consistent with the explanation provided here.

4.4. Possible solutions to eliminate polygonal wheels

According to the analyses above, the development of polygonal wheels comes from three interactive conditions. They are initial 4th order polygonal wheel, the natural frequency of the linear motor and the vehicle speed. Thereby, the mitigating solutions could be proposed from three aspects.

(1) Adjusting the natural frequencies of the linear motor: The suspension parameters and mass properties of the linear motor determine its natural frequencies. Increasing the vertical stiffness of rubber components in the rods suspending the linear motor by 150% would result in an increase of the linear motor natural frequency by approximately 22.5% and avoid the resonance of the motor in the speed range from 0 to 90km/h. (2) Adjusting speeds: Changing the vehicle speed has limited effects if the resonance speed cannot be avoided in real operational service. However, reducing the time spent by the vehicle travelling in the resonance speed range can still alleviate the polygonal wear. (3) Improving the wheel re-profiling technology: Re-profiling machine and process could be improved to reduce initial wheel irregularity.

5. New strategies for investigating wheel polygonization

The exploration of the case study inspires new strategies for investigating wheel polygonization, which could be applied generally in other types of railway vehicles.

(1) Identifying resonance speed(s)

Speed is an extremely important factor when polygonal wear is investigated since it determines the frequency of wheel excitation. In analyses for the metro vehicle, a resonance speed is identified through simulation and validated by field tests. Identifying a resonance speed points the investigation towards a specific frequency range, facilitating a better

understanding of the causes of polygonal wear and the search for remedies. An approach to identify this speed could be testing dynamic behaviours of vehicles at varying speeds. A simulation example to identify the resonance speed for the metro vehicle can be seen in Figure 24. In this simulation, an initial 4th polygon order and increasing speed are applied and the resonance speed is identified by looking for peaks of the ride index.

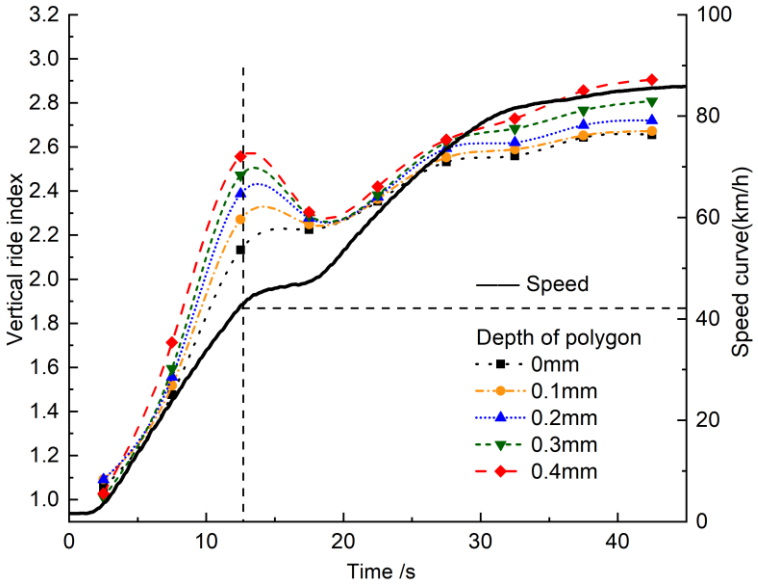

Figure 24 *Resonance speed identification in varying speeds*

(2) Dividing the development of polygonal wear into phases

In the case study for the metro vehicle, the long-term field tests validate that the dynamic behaviours of the vehicle have different features in different stages. The polygonal wear simulation also shows that the wear evolution in different phases has different wear patterns. We divide the polygonal wear evolution into two phases as shown in Figure 25. In phase 2, the wear pattern tends to a stable waveform and only grown in amplitude. Instead, the essential process determining the order of polygon occurs in phase 1. However, when wheel polygonization is observed, the studies usually started with phase 2 which may provide very useful insight on the mechanisms of wear depth growth, but the evolution in the waveform of polygonal wear in phase 1 is disregarded.

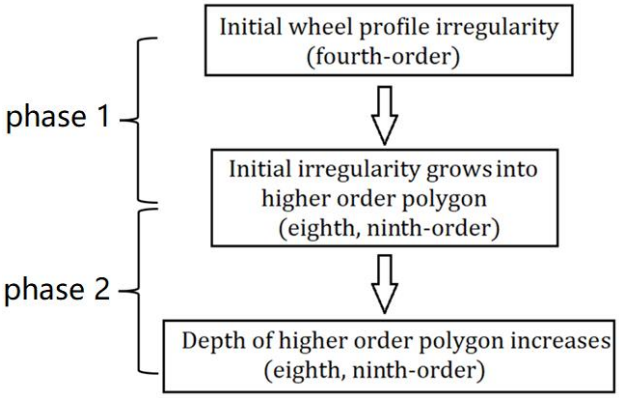

Figure 25 *Developing phases of polygonal wear*

6. Conclusions

In this work, a long-term iterative wear model is proposed to study the evolution of the polygonal wear. Integration steps, curve fitting methods and wheel profile updating strategy are three crucial factors that will affect the accuracy of the simulation. Through the wear model, the evolution of polygonal wear is studied quantitatively providing an effective approach to investigate the mechanism of wheel polygonization. The results of numerical investigations are shown in the

paper to be consistent with measurements from line tests and support the conclusion for the case study that the process of formation and growth of polygonal wear consists of two phases: a first one in which an initial small amplitude 4^{th} order out of roundness evolves in a corrugation profile where 8^{th} and 9^{th} order polygons are dominating, and a second one in which the amplitude of polygonal wear keeps growing without significant changes in the waveform. Both phases are profoundly affected by the excitation of resonances in the vehicle, particularly in the linear motor and wheelsets, resulting in intense resonance effects at some speeds.

Apart from the reason explained in this work, some other factors could contribute to the evolution of polygonal wear to some extent. High-frequency vibration of the track is not considered in this paper but could play a role, especially when high-order polygonal wear has developed and particularly for the case of high-speed trains where excitation frequencies are higher. These factors could be analysed in future developments of this work.

Future extensions of this work can also be addressed to assessing the effect of using a more accurate "local wear" model instead of the "global wear" model used in this paper, although this would increase substantially the computational effort required, and to considering other models for wheel/rail contact as an alternative to FASTSIM.

Finally, further comparison with measurements from line tests, especially increasing the frequency of wheel profile measurements during the phase of polygonal wear development would allow a more thorough validation of the model and of the proposed two-phase mechanism for polygonal wear proposed in the paper.

References

[1] X. Jin, L. Wu, J. Fang, S. Zhong, and L. Ling, An investigation into the mechanism of the polygonal wear of metro train wheels and its effect on the dynamic behaviour of a wheel/rail system, *Veh. Syst. Dyn.*, vol. 50, no. 12, pp. 1817–1834, 2012. DOI: 10.1080/00423114.2012.695022

[2] B. Fu, S. Bruni, and S. Luo, Numerical simulation for polygonal wear of railway wheels, in *Proceedings of the 11th International Conference on Contact Mechanics and Wear of Rail/wheel Systems, CM 2018*, 2018.

[3] B. Morys, Enlargement of out-of-round wheel profiles on high speed trains, *J. Sound Vib.*, vol. 227, no. 5, pp. 965–978, 1999. DOI: 10.1006/jsvi.1999.2055

[4] A. Johansson and C. Andersson, Out-of-round railway wheels - A study of wheel polygonalization through simulation of three-dimensional wheel-rail interaction and wear, *Veh. Syst. Dyn.*, vol. 43, no. 8, pp. 539–559, 2005. DOI:10.1080/00423110500184649

[5] G. Tao, L. Wang, Z. Wen, Q. Guan, and X. Jin, Experimental investigation into the mechanism of the polygonal wear of electric locomotive wheels, *Veh. Syst. Dyn.*, vol. 56, no. 6, pp. 883–899, 2018. DOI: 10.1080/00423114.2017.1399210.

[6] A. Johansson, Out-of-round railway wheels-assessment of wheel tread irregularities in train traffic, *J. Sound Vib.*, vol. 293, no. 3–5, pp. 795–806, 2006. DOI: 10.1016/j.jsv.2005.08.048

[7] A. Johansson, J.C.O. Nielsen. Out-of-round railway wheels—wheel—rail contact forces and track response derived from field tests and numerical simulations*Proc. Inst. Mech. Eng. Part F J. Rail Rapid Transit*, 2003, vol. 217, no.2, pp.135-146. 2003. DOI: 10.1243/095440903765762878.

[8] D. W. Barke and W. K. Chiu, A review of the effects of out-of-round wheels on track and vehicle components, *Proc. Inst. Mech. Eng. Part F J. Rail Rapid Transit*, vol. 219, no. 3, pp. 151–175, 2005. DOI: 10.1243/095440905X8853

[9] J. ZHANG and X. JIN, Effect of the first two wheelset bending modes on wheel-rail contact behavior, *J. Zhejiang Univ. Sci. A*, vol. 15, no. 12, pp. 1002–1018, 2014.DOI: 10.1631/jzus.a1400233

[10] M. Meywerk, Polygonalization of railway wheels, *Arch. Appl. Mech.*, vol. 69, no. 2, pp. 105–120, 1999. DOI: 10.1007/s004190050208

[11] K.Popp , H. Kruse and I. Kaiser. Vehicle-Track Dynamics in the Mid-Frequency Range, *Veh. Syst. Dyn.*, vol. 31, no.5-6, pp. 423-464. 1999. DOI: 10.1076/vesd.31.5.423.8363.

[12] J. F. Archard, Contact and rubbing of flat surfaces, *J. Appl. Phys.*, vol. 24, no. 8, pp. 981–988, 1953.DOI: 10.1063/1.1721448

[13] F. Braghin, S. Bruni, and F. Resta, Wear of Railway Wheel Profiles: A Comparison between Experimental Results and a Mathematical Model, *Veh. Syst. Dyn.*, vol. 37, no. sup1, pp. 478–489, 2003. DOI: 10.1080/00423114.2002.11666256

[14] J. C. O. Nielsen, R. Lundén, A. Johansson, and T. Vernersson, Train-Track Interaction and Mechanisms of Irregular Wear on Wheel and Rail Surfaces, Veh. Syst. Dyn., vol. 40, no. 1–3, pp. 3–54, 2003. DOI: 10.1076/vesd.40.1.3.15874

[15] B. Peng, S. Iwnicki, P. Shackleton, Y. Zhao, and D. Cui. A practical method for simulating the evolution of railway wheel polygonalization. 25th international symposium on dynamics of vehicles on roads and tracks, Rockhampton, Australia, July,2017.

[16] W. Cai, M,Chi, X,Wu, A study of the mechanism of high order wheel polygonal wear. 11th international conference on contact mechanics and wear of rail/wheel system 2018. Delft, the Netherlands, September,2018.

[17] P. Meinke and S. Meinke, Polygonalization of wheel treads caused by static and dynamic imbalances,"*J. Sound Vib.*, vol. 227, no. 5, pp. 979–986, 1999. DOI: 10.1006/jsvi.1999.2590[1]

[18] T. B. Meinders, P. Meinke, and W. O. Schiehlen, Wear estimation in flexible multibody system with application to railroads. Multibody dynamics 2005, Eccomas Thematic Conference. Madrid Spain, June 2005.

[19] R.Luo, J.Zeng ,P.Wu, H.Dai. Simulation and Analysis of Wheel Out-of-roundness Wear of High-speed Train. Journal of the China railway society. Vol.32, no.5, pp.30-35, 2010,DOI:10.3969/j.issn.1001-8360.2010.05.006.

[20] J. Pombo *et al.*, "Development of a wear prediction tool for steel railway wheels using three alternative wear functions," *Wear*, vol. 271, no. 1–2, pp. 238–245, 2011.DOI: 10.1016/j.wear.2010.10.072

[21] C. Boor, A Practical Guide to Splines (Revised Edition). Springer. Madison, USA, 2001

[22] B. Fu, S. Luo, Z. Xu, Y. Tang, and W. Ma, Effects of the vibration characteristics of linear motors on the polygon wheel problem, Zhendong yu Chongji/Journal Vib. Shock, vol. 37, no. 1, 2018.DOI: 10.13465/j.cnki.jvs.2018.01.023

[23] D. Cui et al., Effect of the turning characteristics of underfloor wheel lathes on the evolution of wheel polygonisation, Proc. Inst. Mech. Eng. Part F J. Rail Rapid Transit, vol. 233, no. 5, pp. 479–488, 2019. DOI: 10.1177/0954409718795760

[24] Mechanical vibration and shock - Evaluation of human exposure to whole body vibration -Part 1: General requirements. ISO 2631-1, International Organization for Standardization, Genève, 1997

[25] K. Knothe and S. Stichel, *Rail Vehicle Dynamics*. Springer, Stockholm, Sweden 2016.

[26] A. Johansson, Out-of-round railway wheels-assessment of wheel tread irregularities in train traffic, J. Sound Vib., vol. 293, no. 3–5, pp. 795–806, 2006.

[27] M. Shi, W. Li, M. Wu, and G. Shen, Analysis of Out-of-Round Wheels and the Effect of Wheel Polygonalization on Vehicle Vibration, *11th Int. Conf. CONTACT Mech. WEAR RAIL/WHEEL Syst. DELFT, NETHERLANDS, Sept. 24-27, 2018*, vol. 17, pp. 856–861, 2018.